Determination of the heat of formation of O_3 using vacuum ultraviolet laser-induced fluorescence spectroscopy and two-dimensional product imaging techniques

Nori Taniguchi, Kenshi Takahashi, and Yutaka Matsumi[a)]
Solar-Terrestrial Environment Laboratory and Graduate School of Science, Nagoya University, Honohara 3-13, Toyokawa, Aichi 442-8507, Japan

Scott M. Dylewski
Department of Applied Physics, Cornell University, Ithaca, New York 14853

Joseph D. Geiser and Paul L. Houston
Department of Chemistry and Chemical Biology, Cornell University, Ithaca, New York 14853

(Received 7 June 1999; accepted 19 July 1999)

Two different techniques, vacuum ultraviolet laser-induced fluorescence (VUV-LIF) spectroscopy and two-dimensional (2D) ion counting product imaging, have been used to determine the bond energy for the dissociation of jet-cooled O_3 into $O(^1D)+O_2(a\ ^1\Delta_g)$. The photofragment excitation (PHOFEX) spectrum for $O(^1D)$ products is recorded by detecting the VUV-LIF signal associated with the $3s\ ^1D^0-2p\ ^1D$ transition at 115.22 nm while scanning the photolysis laser wavelength between 305 and 313 nm. A clear cut-off corresponding to the appearance threshold into $O(^1D)+O_2(a\ ^1\Delta_g)$ is observed in this PHOFEX spectrum. The 2D image of the $O(^1D)$ products from the O_3 photolysis near 305 nm is measured using an ion-counting method, with the detection of $O(^1D)$ atoms by [2+1] resonance enhanced multiphoton ionization (REMPI) at 205.47 nm. The kinetic-energy distribution obtained from the 2D image shows rotational structure due to the $O_2(a\ ^1\Delta_g, v''=0)$ fragment. The bond energy into $O(^1D)+O_2(a\ ^1\Delta_g)$ has been obtained from the rotational assignments in the kinetic-energy distribution. The two different experimental approaches give consistent results and an accurate value of the bond dissociation energy into $O(^1D)+O_2(a\ ^1\Delta_g)$ is found to be 386.59 ± 0.04 kJ/mol. The standard heat of formation of O_3, $\Delta_f H^0(O_3)=-144.31\pm0.14$ kJ/mol, has also been calculated from the bond energy obtained, in conjunction with thermochemical data for O_2 molecule and O atom. The uncertainty for the $\Delta_f H^0(O_3)$ value obtained in the present study is smaller than the previous value which has been used widely. © *1999 American Institute of Physics.* [S0021-9606(99)02338-7]

I. INTRODUCTION

The photochemistry and thermochemistry of O_3 is atmospherically and fundamentally interesting. For example, photodissociation of O_3 by ultraviolet radiation plays a key role in atmospheric chemistry.[1] There are five energetically possible fragmentation pathways in the near UV photolysis of O_3:

$$O_3+h\nu(\lambda<310\ \text{nm})\rightarrow O(^1D)+O_2(a\ ^1\Delta_g), \quad (1)$$

$$O_3+h\nu(\lambda<411\ \text{nm})\rightarrow O(^1D)+O_2(X\ ^3\Sigma_g^-), \quad (2)$$

$$O_3+h\nu(\lambda<463\ \text{nm})\rightarrow O(^3P)+O_2(b\ ^1\Sigma_g^+), \quad (3)$$

$$O_3+h\nu(\lambda<612\ \text{nm})\rightarrow O(^3P)+O_2(a\ ^1\Delta_g), \quad (4)$$

$$O_3+h\nu(\lambda<1180\ \text{nm})\rightarrow O(^3P)+O_2(X\ ^3\Sigma_g^-), \quad (5)$$

where the long wavelength limits given in parentheses indicate the thermodynamic threshold for the fragmentations in the case that the parent $O_3(X\ ^1A_1)$ molecule is excited from its vibrationless level ($v''=0$).[2,3] Considerable experimental effort has been made to investigate the photodissocation processes of O_3 in the UV (ultraviolet) region[4–24] and it has turned out that channels (1) and (5) are predominant in the Hartley band photodissociation at $\lambda<305$ nm, with reported quantum yields of 0.9 and 0.1, respectively.[3] However, recent experiments confirmed that spin-forbidden channels (2)–(4) as well as spin-allowed channels (1) and (5) occur in the Huggins band.[13–24] The principal photodissociation process in the Huggins band at $\lambda>310$ nm is channel (5). At wavelengths longer than 310 nm, which is the thermochemical threshold wavelength for channel (1), non-negligible production of the $O(^1D)$ atoms has been observed and attributed to the channel (1) photodissociation of internally excited O_3 and the spin-forbidden dissociation of channel (2).[13–22]

Accurate values of the dissociation energies are important for establishing the heat of formation of chemical species. They are also central to dynamical studies of the quantum state distributions of the nascent photofragments, since they define the available energy in the photodissociation reaction. The JANAF thermochemical tables[25] list the value of -145.348 ± 1.7 kJ/mol for $\Delta_f H^0(O_3)$ at 0 K. The bond dissociation energy of $D_0(O(^3P)-O_2(X\ ^3\Sigma_g^-))=101.4\pm1.7$ kJ/mol has been widely used for many studies: For example,

a)Electronic mail: matsumi@stelab.nagoya-u.ac.jp

photofragment kinetic-energy studies,[4–12] determination of bond energies for other molecules,[26] and comparison with theoretical calculations of O_3 electronic states, etc.[27,28] The value in the JANAF table is based on old calorimetric measurements in 1910 and 1932.[29,30] The value of $\Delta_f H^0(O_3)$ is important in atmospheric chemistry as well as in industries and physical chemistry. For example, estimations of the equilibrium conditions in chemical reactions involving O_3 are dependent on the $\Delta_f H^0(O_3)$ value. Therefore, we have remeasured $\Delta_f H^0(O_3)$ using newly developed and more accurate techniques.

$O(^1D)$ and $O(^3P_j)$ atoms have one-photon absorption only in the VUV region. Detection of those oxygen atoms by a laser-induced fluorescence technique in the vacuum ultraviolet region (VUV-LIF) is a powerful tool to study photodissociation and collisional reactions in which $O(^1D)$ or $O(^3P_j)$ atoms are involved. Recently, Takahashi *et al.*[14–17] have studied the O_3 photolysis and measured the quantum yields of $O(^1D)$ production as a function of temperature and photolysis wavelength. Measurement of kinetic energy release and spatial angular distribution of the $O(^1D)$ and $O(^3P)$ fragments from the UV photolysis of O_3 was also performed.[6,12] In those studies, the $O(^1D)$ and $O(^3P)$ atoms produced in the O_3 photolysis were directly detected by the VUV-LIF technique. Since the technique was highly sensitive, they could measure the $O(^1D)$ and $O(^3P_j)$ atoms with low pressure of O_3 and short delay time between the photolysis and probe lasers, so that secondary reactions could be safely ignored.

The 2D product imaging technique allows us to extract simultaneously the kinetic-energy and angular distributions of a state-selected product from chemical reactions.[7,11,31–35] In this technique, products from a photodissociation reaction are ionized, and their velocity is imaged by accelerating the ions into a detector formed by a pair of microchannel plates (MCP) and a fluorescent screen. The positions of the ions are related to their speed and angular distribution in the center-of-mass frame. Despite the success of 2D ion imaging in many fields of physical chemistry, the potential of the technique has not been completely exploited because several factors such as background noise and detector resolution have affected the performance. A very recent study by Chang *et al.*[34] has presented an ion-counting method that significantly improves the spatial resolution and detection sensitivity of 2D product imaging. The method results in a further increase by a factor of ~5 in resolution over the technique of the velocity map imaging developed by Eppink and Parker.[35] The high resolution velocity mapping—ion counting technique enables us to obtain precise and accurate bond energies in photolysis experiments.

In this paper, we report an accurate value for the energy threshold of reaction channel (1). The two different experimental approaches, which are the VUV-LIF detection of the $O(^1D)$ atoms and the 2D product imaging techniques, have been carried out to reveal the accurate channel (1) dissociation energy. The photofragment excitation (PHOFEX) spectra for $O(^1D)$ from the photolysis of jet-cooled O_3 are measured by monitoring the VUV-LIF signal while scanning the photolysis laser wavelength around the threshold for channel (1) ($\lambda \sim 310$ nm). The accurate threshold wavelength for channel (1) is obtained from the clear cut-off in the PHOFEX spectrum for $O(^1D)$. Takahashi *et al.*[16] previously reported the threshold wavelength of channel (1) using the VUV-LIF technique in a supersonic free-jet. We find that their experiments may have had a problem with the rotational cooling of parent O_3 molecules in the supersonic free-jet. In the present study, we report a revised value for the channel (1) threshold wavelength. We also obtain the bond energy into $O(^1D)+O_2(a\ ^1\Delta_g)$ from the kinetic-energy distributions of the 2D ion image of $O(^1D)$. The bond energy obtained by the 2D imaging technique is in good agreement with the threshold wavelength obtained by the VUV-LIF technique in this work. The heat of formation for O_3, $\Delta H_f^0(O_3)$, is also calculated, in conjunction with the available data for the O_2 molecule and the O atom.

II. EXPERIMENT

A. Vacuum-ultraviolet laser-induced fluorescence spectroscopy

Two different experimental apparatuses, one at Nagoya University and the other at Cornell University, were used in the present study. The Nagoya apparatus is the vacuum ultraviolet laser-induced fluorescence detection system of the atomic oxygen fragments and has been applied previously to the study ozone photochemistry.[6,12,14–17] Details have been described elsewhere[6,14] and here only brief details pertinent to the current study are described. The O_3 photolysis was studied under conditions of substantial cooling in a pulsed expansion to suppress the contribution from the photodissociation of internally excited parent O_3 molecules. The gas mixture (typically 2% to 3% O_3 in helium, at a total pressure of ~1000 Torr) was injected through a pulsed nozzle (General Valve, Series 9, hole diam. 0.8 mm) into the stainless steel vacuum chamber, evacuated by a liquid–nitrogen trapped oil diffusion pump.

For the photolysis light source, a dye laser pumped by a Nd:YAG laser (Lambda Physik, SCANmate 2EY-400) was used with the mixture solution of Rhodamine B and Rhodamine 101 laser dyes. The visible output from the dye laser was frequency doubled in a KD*P crystal to generate the tunable UV photolysis beam between 305 and 313 nm. The incident photolysis laser intensity was typically 0.5–1 mJ/pulse. The wavelength of the fundamental visible light was calibrated by simultaneously measuring the laser-induced fluorescence excitation spectrum of I_2 vapor and comparing it with published data.[36] The spectral linewidth of the fundamental laser light was estimated to be 0.10 cm^{-1} from the linewidths of the I_2 spectrum.

The $O(^1D)$ photofragments from the O_3 photolysis was detected by the VUV-LIF technique at 115.22 nm which is resonant with the $3s\ ^1D^0-2p\ ^1D$ transition. The 115.22 nm laser light was generated by phase-matched frequency tripling of the output from a dye laser at 345.6 nm in xenon (40 Torr)/argon (120 Torr) gas mixture.[37] A dye laser pumped by a XeCl excimer laser (Lambda Physik, FL3002E and Lextra-50) was used with PTP dye in 1,4-dioxane solvent to generate the 345.6 nm light (~5 mJ/pulse). The 345.6 nm radia-

tion was focused with a lens ($f=200$ mm) into a Xe/Ar gas containing cell. The VUV laser light generated was introduced into a reaction chamber through a LiF window. A small percentage of the VUV radiation was reflected into a gas cell of nitric oxide (NO) by a LiF window held in the vacuum chamber. The relative VUV laser intensity was monitored by the photoionization current of the NO gas.

Photofragment excitation (PHOFEX) spectra for $O(^1D)$ were recorded by tuning the probe laser wavelength to the center of the $O(^1D)$ absorption resonance and scanning the photolysis laser wavelength. The pump and probe laser pulses were separated in time by 100 ns, which was controlled by a pulse generator (Stanford Research, DG535). The VUV-LIF signal was detected by a solar-blind photomultiplier tube (EMR, 541J-08-17). The detection axis was orthogonal to propagation directions of both VUV probe and photodissociation laser beams. The output from the photomultiplier was fed into a gated integrator (Stanford Research, SR-250).

B. Two-dimensional (2D) product imaging using the ion-counting method

The Cornell apparatus for product imaging experiments has been described more fully elsewhere.[31,34] A molecular beam of ozone was formed by flowing helium with about 810 Torr backing pressure over O_3 maintained on silica gel at a temperature of -78 °C. The subsequent mixture of $<1\%$ ozone was expanded through a pulsed 250 μm diameter nozzle and collimated by a 500 μm diameter skimmer mounted about 5 mm from the nozzle orifice. Further downstream, the molecular beam was crossed at right angles by two counter-propagating laser beams, one serving to dissociate the ozone and the other to probe the resulting $O(^1D)$ fragments using the $O(^1P_1 \leftarrow\leftarrow {}^1D_2)$ [2+1] REMPI scheme at 205.47 nm.[38] The wavelength of this probe laser was scanned over the Doppler width of the $O(^1D)$ fragments.

The photolysis laser wavelength of 305.746 nm was produced by frequency doubling the output of an optical parametric oscillator (Spectra-Physics MOPO-730) pumped by an injection seeded Nd:YAG laser (Spectra Physics GCR-230). Typical laser powers were 2 mJ/pulse with a pulse duration of 8–10 ns. The photolysis wavelength was calibrated by the optogalvanic effect in neon. The 205.47 nm ionizing laser radiation was generated by frequency doubling the output of an injection-seeded Nd:YAG-pumped dye laser and then summing this doubled light with the remaining fundamental. Typical powers achieved were 1 mJ/pulse with a pulse duration of 8–10 ns. Both lasers were operated at 10 Hz. The polarizations of both the photolysis and probe laser beams were perpendicular to the plane defined by the molecular and laser beams.

The velocity mapping-ion counting technique[34,35] was used to obtain high resolution photofragment images. An electrostatic lens was employed that served both to extract the ionized $O(^1D)$ fragments from the interaction zone and to de-blur the image. The magnification factor of this electrostatic lens was measured to be 1.17 ± 0.02 by dissociating O_2 and detecting the $O(^3P_2)$ fragment using the $O(3p\ ^3P_{2,1,0} \leftarrow\leftarrow 2p\ ^3P_2)[2+1]$ REMPI scheme at 226.23 nm.[39,40] The ionized fragments were accelerated into a flight tube mounted along the axis of the molecular beam. The ions were imaged by a position sensitive detector consisting of a chevron double micro-channel plate (MCP) assembly coupled to a fast phosphor screen. The image on the phosphor screen was recorded by a 640×480 pixel charge coupled device (CCD) camera. Both the MCP and CCD camera were electronically shuttered to collect signal corresponding to the mass of the oxygen atoms.

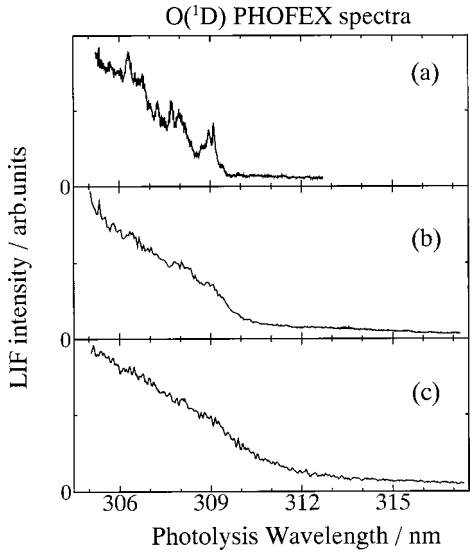

FIG. 1. Photofragment excitation (PHOFEX) spectra for $O(^1D)$ photoproducts from the photolysis of O_3 under jet-cooled and bulb conditions. The PHOFEX spectra were recorded by detecting the vacuum ultraviolet (VUV) laser-induced fluorescence intensity of the $O(^1D)$ atoms during the scan of the photolysis laser wavelength between 305 and 313 nm. (a) PHOFEX spectrum for $O(^1D)$ photoproducts recorded under jet-cooled conditions in the present study. (b) PHOFEX spectrum under jet-cooled conditions previously presented by Takahashi *et al.* (Ref. 16). (c) PHOFEX spectrum in a flow cell at room temperature, which is taken from the report by Takahashi *et al.* (Ref. 17).

III. RESULTS AND DISCUSSION

Figure 1 shows the PHOFEX spectra of $O(^1D)$ fragments produced in the photolysis of O_3. The PHOFEX spectra were measured by scanning the photolysis laser wavelength when the wavelength of the VUV probe laser was tuned to the $3s\ ^1D^0-2p\ ^1D$ resonance line at 115.22 nm. Figure 1(a) is the PHOFEX spectrum obtained under the supersonic free-jet conditions in the present study. For comparison, the previously measured PHOFEX spectrum under the supersonic free-jet conditions[16] is shown in Fig. 1(b). The PHOFEX spectrum in a flow cell at room temperature is also shown in Fig. 1(c), which is taken from the report by Takahashi *et al.*[17] Doppler line shapes of the nascent $O(^1D)$ atoms produced in the O_3 photolysis were measured at several points in the photolysis wavelength range of Fig. 1 by scanning the probe VUV laser wavelength. The Doppler profiles measured were independent of the photolysis wavelength. The width of all the Doppler profiles were measured to be 0.65 cm^{-1}, which is almost identical with the laser band width. This indicates that the $O(^1D)$ atoms from the O_3 photolysis in this wavelength range are predominantly pro-

duced via channel (1), since the excess energy for channel (1) is small near the threshold and the $O(^1D)$ atoms produced in the dissociation have small translational energy. The $O(^1D)$ PHOFEX spectra measured were corrected for UV photolysis and VUV probe laser intensity variations. The PHOFEX spectra shown in Fig. 1 corresponds to the relative $O(^1D)$ yield spectra.

A clear cut-off as well as distinct structures is recognized in the jet-cooled $O(^1D)$ PHOFEX spectrum in Fig. 1(a). The distinct structures may correlate to vibrational levels in the upper electronic state of O_3. The cut-off wavelength should correspond to an appearance potential of the dissociation path into $O(^1D)+O_2(^1\Delta_g)$, that is, channel (1) for vibrationless O_3 molecules. To obtain an accurate value of the threshold wavelength for channel (1), the degree of the rotational excitation in parent O_3 molecules must be taken into account. The VUV-LIF spectrum of jet-cooled carbon monoxide (CO) molecules at around 115 nm was measured under the same jet conditions as used in the O_3 experiments. The VUV-LIF spectrum of CO is associated with the (0,0) band of the $B\,^1\Sigma^+-X\,^1\Sigma^+$ system.[41] A Boltzmann distribution at a rotational temperature of $T_{\rm rot}=3$ K fit the rotational profiles in the CO excitation spectra quite well. Similar rotational cooling is expected to be achieved in the present O_3 experiments. In contrast to the PHOFEX spectrum in free-jets [Fig. 1(a)], the PHOFEX spectrum in the flow cell at room temperature [Fig. 1(c)] exhibits very smooth variation and the threshold wavelength is not seen clearly. This is due to the rotational excitation of thermal parent O_3 molecules. The PHOFEX spectrum in the free-jets reported in the previous study by Takahashi *et al.*[16] [Fig. 1(b)] also has less distinct structure than that in the present study [Fig. 1(a)]. This lack of resolution is indicative that the O_3 molecules in the previous study were not well cooled in the supersonic free-jets. In the present study, we have measured the PHOFEX spectra under various nozzle conditions. We have found that the resolution of the structures in the PHOFEX spectra strongly depends on the stagnation pressure of the free-jets and on the distance between the nozzle and the laser beams. The PHOFEX spectra under low stagnation pressure conditions and/or at short nozzle-beam distances had less well resolved structures yielding spectra similar to that in the previous study [Fig. 1(b)]. Therefore, we suspect that the rotational cooling in the free-jets for the measurements of the PHOFEX spectra around the threshold was not well-performed and that the rotational temperature of the parent O_3 molecules was relatively high in the previous study.[16]

Figure 2 shows the detailed PHOFEX spectrum of the $O(^1D)$ atoms produced in the photolysis of O_3 under jet-cooled conditions in the wavelength range of 309.15–309.65 nm. For calibration of the photolysis laser wavelength, fluorescence excitation spectra of I_2 molecules around 620 nm were simultaneously recorded, which is also shown in Fig. 2. For the I_2 spectra measurements, a few percent of the fundamental light from the photolysis laser was reflected into the I_2 containing cell by a thin quartz plate. The photolysis laser wavelength was calibrated by making a comparison between the measured I_2 spectra and the published spectral data.[36] The average energy ($=\frac{3}{2}\,kT$) of the rotational excitation at

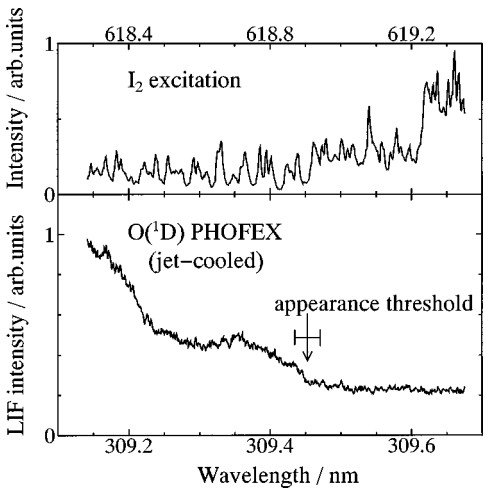

FIG. 2. Detailed photofragment excitation (PHOFEX) spectrum for $O(^1D)$ photoproducts from the photolysis of jet-cooled O_3 in the wavelength range of 309.15–309.65 nm. Fluorescence excitation spectrum of I_2 vapor is also shown, which was simultaneously measured with the PHOFEX spectrum measurements. The I_2 spectrum is used to calibrate the fundamental wavelength of the dye laser used as the photolysis radiation. The cut-off wavelength corresponds to the thermochemical energy threshold of the reaction $O_3+h\nu\rightarrow O(^1D)+O_2(a\,^1\Delta_g)$. The threshold wavelength is determined to be 309.45 ± 0.03 nm.

$T_{\rm rot}=3$ K is 3 cm^{-1} (0.04 kJ/mol), which corresponds to the wavelength shift of 0.03 at 310 nm. Taking the rotational excitation into account, the cut-off wavelength was determined to be 309.45 ± 0.03 nm for rotationless and vibrationless O_3 molecules, as shown in Fig. 2. This cut-off wavelength corresponds to the appearance potential for the dissociation path into $O(^1D)+O_2(\,^1\Delta_g)$ [channel (1)]. From the threshold wavelength of 309.45 ± 0.03 nm, the bond energy of O_3 dissociating into channel (1) was calculated to be 386.58 ± 0.04 kJ/mol. The threshold wavelength value determined from the present PHOFEX measurements is slightly shorter than the value of 310.2 ± 0.2 nm in the previous measurements.[16]

The background production of $O(^1D)$ from the jet-cooled O_3, which continues even at wavelengths longer than the threshold wavelength, is observed in the $O(^1D)$ PHOFEX spectrum, as shown in Figs. 1 and 2. Formation of the $O(^1D)$ atoms at $\lambda>309.45$ nm was also observed in the flow cell experiments at 200–320 K, which was attributed to the contribution from the photodissociation of vibrationally excited parent O_3.[13–22] The vibrationally excited $O_3(X\,^1A_1)$ may survive in the photolysis zone of the free-jet, since vibrational cooling in the jet-cooled sample is slower than rotational cooling.[42]

Figure 3(a) shows a raw image of 2D projection of the $O(^1D)$ fragments, in which the $O(^1D)$ atoms produced from the 305.746 nm photolysis of O_3 were probed by a technique of [2+1] REMPI at 205.47 nm. The probe laser wavelength is resonant with the two-photon transition of $O(^1P_1\leftarrow\leftarrow{}^1D_2)$. The polarization vectors of the photolysis and probe laser light are parallel to the vertical axis of the image in Fig. 3(a). Figure 3(b) shows a slice of the 3D velocity distribution obtained by inverse Abel transform of the raw image shown in Fig. 3(a). The bright inner features result

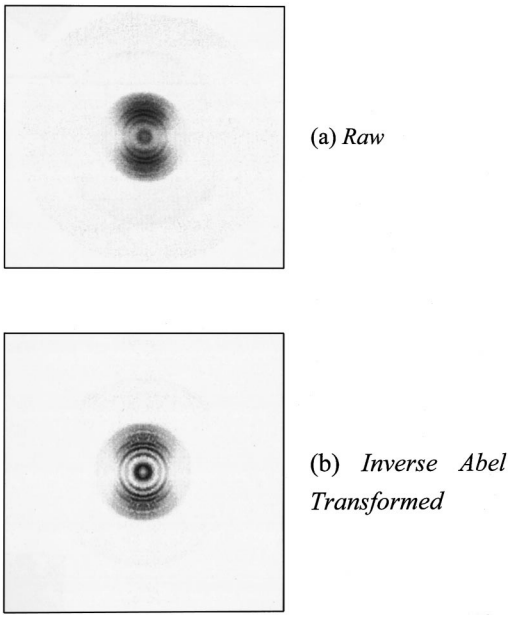

FIG. 3. (a) Raw (unsymmetrized) two-dimensional (2D) image of the $O(^1D)$ photoproducts produced from the photolysis of jet-cooled O_3 at 305.746 nm. The $O(^1D)$ atoms are probed by the technique of resonance enhanced multiphoton ionization (REMPI) at 205.47 nm. The polarization direction of the photolysis and probe laser light is parallel to the vertical line of the figure plane of the image. (b) A slice of the 3D velocity distribution calculated by applying the inverse Abel transform to the raw image of (a).

from the photolysis of O_3 in its ground vibrational state while the outermost feature results from the photolysis of vibrationally hot O_3.

Figure 4 shows the center-of-mass kinetic energy distribution for $O(^1D)$ produced in the photodissociation of O_3 at 305.746 nm, which was calculated from the 3D slice image shown in Fig. 3(b). Energy distributions are obtained by integrating all angles at a given radius, and then converting the radius to a total kinetic energy release of the O_2 and $O(^1D)$ fragments. The resulting intensity distribution for the above images is shown in Fig. 4. The structural peaks in the kinetic-energy distribution correspond to the rotational states of the co-fragments, $O_2(a\,^1\Delta_g, v''=0)$, and the rotational

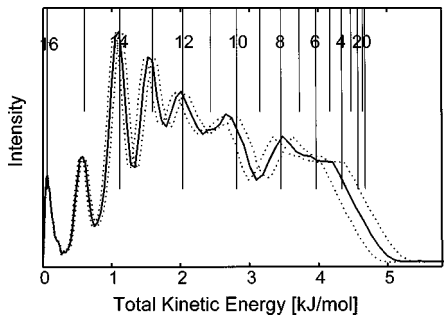

FIG. 4. Center-of-mass kinetic energy distribution of the $O(^1D)$ atoms from the photolysis of jet-cooled O_3 at 305.746 nm, which is calculated from the 3D slice image shown in Fig. 3(b). Structures observed are due to the rotational states distribution of the $O_2(a\,^1\Delta_g, v''=0, J'')$ fragments. Rotational assignments are calculated using published rotational constants (Ref. 43) and are indicated as a comb. Dotted lines represent the error associated with our measurement. The bond energy of O_3 dissociating into $O(^1D) + O_2(a\,^1\Delta_g)$ is determined to be 386.59 ± 0.03 kJ/mol.

peaks are successfully assigned as indicated in Fig. 4, using the rotational constants of $O_2(a\,^1\Delta_g, v''=0)$ studied by Nigh and Valentini.[43] The bond energy dissociating into channel (1) is calculated to be 386.59 ± 0.03 kJ/mol from the rotational assignments. This corresponds to a wavelength limit of 309.44 ± 0.02 nm.

The main source of error in determining the bond energy from the 2D imaging experiments is the magnification factor of the electrostatic lens. Even though this error may become significant where the kinetic energy of ions is large, the error from the magnification factor is very small at low kinetic energies. Therefore, the value of bond dissociation energy was found by adjusting it so that the rotational assignment at $J''=16$ was centered on the peak so that the area to the right and left of the assignment was equal. Uncertainty of the value of the bond energy was estimated to be about 0.03 kJ/mol from the width of the $J''=16$ peak. A second possible source of error is from the uncertainty of the flight times. However, this source was found to be insignificant as the flight times were measured with an uncertainty of ± 0.02 μs. This gives an error of about 3×10^{-3} kJ/mol at 5 kJ/mol kinetic energy on our plot for 305.746 nm. At the peak assigned to $J''=16$, the error is much smaller: about 8×10^{-4} kJ/mol. These uncertainties are still much smaller than the width of peaks.

Valentini *et al.*[5] measured the internal state distributions of the $O_2(a\,^1\Delta_g)$ fragments produced from the 230–310 nm photolysis of O_3, applying coherent anti-Stokes Raman scattering (CARS) spectroscopy. They observed an apparent propensity for even-J'' states in the rotational state distributions in the $O_2(a\,^1\Delta_g, v''=0-3)$ fragments, and the propensity was discussed in terms of participating potential energy surfaces. The even-J'' states propensity is clearly observed in the present imaging study (Fig. 4), and the aspect gives confidence to our rotational assignment.

To confirm our measurement at 305.746 nm, we took a second set of images at a dissociation wavelength of 309.096 nm. From the rotational assignment, we derived a value of 386.62 ± 0.05 kJ/mol as the bond energy of O_3 dissociating into channel (1). The uncertainty is somewhat larger than that from the 305.746 nm photolysis experiment, since the signal to noise ratio in the $O(^1D)$ images taken at 309.096 nm was lower. This is because the absorption cross section of O_3 is significantly smaller at the longer wavelength, leading to a correspondingly lower signal. The bond energy obtained from the 309.096 nm experiment is in agreement with that from the 305.746 nm experiment within the uncertainties. At both photolysis wavelengths where we took images, we find a steep fall off of the signal occurring near $J''=3$, resulting in very little signal at $J''=0$, 1, and 2. It is likely that the low J'' levels may be less intense since O_3 dissociates from a bent geometry.

The bond energy of O_3 dissociating into channel (1) was determined to be 386.58 ± 0.04 kJ/mol from the PHOFEX spectra measurements, while it was found to be 386.59 ± 0.03 kJ/mol from the 2D ion imaging experiments at 305.746 nm and to be 386.62 ± 0.05 kJ/mol at 309.096 nm. Values obtained from the two different experimental methods are in good agreement with each other within the uncertainties. The

most probable value of the bond energy for channel (1) is thus evaluated to be 386.59 ± 0.04 kJ/mol from the three values obtained. The bond energy value for channel (1) obtained from the present study provides the heat of formation of O_3, $\Delta_f H^0(O_3)$, in conjunction with thermochemical data for O atoms and O_2 molecules. The electronic energy, T_0, of the $O_2(a\,^1\Delta_g)$ state is 7882.39 cm^{-1} (=94.29 kJ/mol).[44] The energy difference between $O(^1D)$ and $O(^3P_2)$ is 15 867.7 cm^{-1} (=189.82 kJ/mol).[45] The errors of these spectroscopic constants are negligible in the calculation of D_0 and $\Delta_f H^0(O_3)$ values. Thus, we can obtain the value for the bond dissociation energy of O_3 into $O(^3P_2)+O_2(X\,^3\Sigma_g^-)$ at 0 K

$$D_0(O(^3P_2)+O_2(X\,^3\Sigma_g^-)) = 102.48 \pm 0.04 \text{ kJ/mol}. \quad (6)$$

Given the standard heat of atomization of O_2 at 0 K is $\Delta_f H^0(O) = (246.79 \pm 0.10)$ kJ mol^{-1} $(\frac{1}{2}O_2 \rightarrow O)$.[25] The standard heat of formation for O_3 at 0 K is derived to be

$$\Delta_f H^0(O_3) = -144.31 \pm 0.14 \text{ kJ/mol (this work)}. \quad (7)$$

The $\Delta_f H^0(O_3)$ value at 0 K, listed in the latest NIST-JANAF thermochemical table,[25] is

$$\Delta_f H^0(O_3) = -145.348 \pm 1.7 \text{ kJ/mol (JANAF table)}. \quad (8)$$

The $\Delta_f H^0(O_3)$ value in the JANAF table is based on old calorimetric measurements performed in 1910 and 1932.[29,30] The uncertainty associated with the $\Delta_f H^0(O_3)$ value reported in the present study is smaller than that listed in the latest JANAF table.

ACKNOWLEDGMENTS

The work at Nagoya was supported by a Grant-in-Aid from the Ministry of Education (Y.M.). The Iwatani Foundation (Y.M.) and the ASAHI BREWERIES Foundation (K.T.) are also acknowledged. The work at Cornell was supported by the National Science Foundation under Grant No. ATM-9528086 and by the Research Institute of Innovative Technology for the Earth Administered by the New Energy and Industrial Technology Development Organization of Japan.

[1] R. P. Wayne, Atmos. Environ. **21**, 1683 (1987).
[2] H. Okabe, *Photochemistry of Small Molecules* (Wiley-Interscience, New York, 1978).
[3] R. Atkinson, D. L. Baulch, R. A. Cox, R. F. Hampson, Jr., J. A. Kerr, M. J. Rossi, and J. Troe, J. Phys. Chem. Ref. Data **26**, 1329 (1997).
[4] R. K. Sparks, L. R. Carlson, K. Shobatake, M. L. Kowalczyk, and Y. T. Lee, J. Chem. Phys. **72**, 1401 (1980).
[5] J. J. Valentini, D. P. Gerrity, D. L. Phillips, J.-C. Nieh, and K. D. Tabor, J. Chem. Phys. **86**, 6745 (1987).
[6] S. M. Shamsuddin, Y. Inagaki, Y. Matsumi, and M. Kawasaki, Can. J. Chem. **72**, 637 (1993).
[7] R. L. Miller, A. G. Suits, P. L. Houston, R. Toumi, J. A. Mack, and A. M. Wodtke, Science **265**, 1831 (1994).
[8] D. Stranges, X. Yang, J. D. Chesko, and A. G. Suits, J. Chem. Phys. **102**, 6067 (1995).
[9] M.-A. Thelen, T. Gejo, J. A. Harrison, and J. R. Huber, J. Chem. Phys. **103**, 7946 (1995).
[10] X. Yang, J. Lin, Y. T. Lee, D. A. Blank, A. G. Suits, and A. M. Wodtke, Rev. Sci. Instrum. **68**, 3317 (1997).
[11] R. J. Wilson, J. A. Mueller, and P. L. Houston, J. Phys. Chem. **101**, 7593 (1997).
[12] K. Takahashi, N. Taniguchi, Y. Matsumi, and M. Kawasaki, Chem. Phys. **231**, 171 (1998).
[13] S. M. Alder-Golden, E. L. Schweitzer, and J. I. Steinfeld, J. Phys. Chem. **76**, 2201 (1982).
[14] K. Takahashi, Y. Matsumi, and M. Kawasaki, J. Phys. Chem. **100**, 4084 (1996).
[15] K. Takahashi, M. Kishigami, Y. Matsumi, M. Kawasaki, and A. J. Orr-Ewing, J. Chem. Phys. **105**, 5290 (1996).
[16] K. Takahashi, M. Kishigami, N. Taniguchi, Y. Matsumi, and M. Kawasaki, J. Chem. Phys. **106**, 6390 (1997).
[17] K. Takahashi, N. Taniguchi, Y. Matsumi, M. Kawasaki, and M. N. R. Ashfold, J. Chem. Phys. **108**, 7161 (1998).
[18] S. M. Ball, G. Hancock, S. E. Martin, and J. C. Pinot de Moira, Chem. Phys. Lett. **264**, 531 (1997).
[19] W. Denzer, G. Hancock, J. C. Pinot de Moira, and P. L. Tyley, Chem. Phys. Lett. **280**, 496 (1997).
[20] W. Denzer, G. Hancock, J. C. Pinot de Moira, and P. L. Tyley, Chem. Phys. **231**, 109 (1998).
[21] R. K. Talukdar, C. A. Longfellow, M. K. Gilles, and A. R. Ravishankara, Geophys. Res. Lett. **25**, 143 (1998).
[22] A. R. Ravishankara, G. Hancock, M. Kawasaki, and Y. Matsumi, Science **280**, 60 (1998).
[23] P. O'Keeffe, T. Ridley, S. Wang, K. P. Lawley, and R. J. Donovan, Chem. Phys. Lett. **298**, 368 (1998).
[24] P. O'Keeffe, T. Ridley, K. P. Lawley, R. R. J. Maier, and R. J. Donovan, J. Chem. Phys. **110**, 10803 (1999).
[25] M. W. Chase, Jr., NIST-JANAF Thermochemical Tables, Fourth Edition, J. Phys. Chem. Ref. Data Monogr. **9**, 1 (1998).
[26] J. L. Gole and R. N. Zare, J. Chem. Phys. **57**, 5331 (1972).
[27] A. Banishevich, S. D. Peyerimhoff, and F. Grein, Chem. Phys. **178**, 155 (1993).
[28] T. Tsuneda, H. Nakano, and K. Hirao, J. Chem. Phys. **103**, 6250 (1995).
[29] A. Kailen and S. Jahn, Z. Anorg. Chem. **68**, 243 (1910).
[30] P. Günther, W. Wassmuth, and L. A. Schryver, Z. Phys. Chem. (Leipzig) **158**, 297 (1932).
[31] D. W. Chandler and P. L. Houston, J. Chem. Phys. **87**, 1445 (1987).
[32] P. L. Houston, Acc. Chem. Res. **22**, 309 (1989).
[33] P. L. Houston, J. Phys. Chem. **100**, 12757 (1996).
[34] B.-Y. Chang, R. C. Hoetzlein, J. A. Mueller, J. D. Geiser, and P. L. Houston, Rev. Sci. Instrum. **69**, 1665 (1998).
[35] A. T. J. B. Eppink and D. H. Parker, Rev. Sci. Instrum. **68**, 3477 (1997).
[36] S. Gerstenkorn and P. Luc, *Atlas du Spectre D'Absorption de la Molecule D'Iode*; C.N.R.S.: Paris, 1978.
[37] R. Hilbig and R. Wallenstein, Appl. Opt. **21**, 913 (1982).
[38] S. T. Pratt, P. M. Dehmer, and J. L. Dehmer, Phys. Rev. A **43**, 4702 (1991).
[39] D. J. Bamford, L. E. Jusinski, and W. K. Bischel, Phys. Rev. A **34**, 185 (1986).
[40] D. J. Bamford, M. J. Dyer, and W. K. B. Bischel, Phys. Rev. A **36**, 3497 (1987).
[41] H. Rottke and H. Zacharias, Opt. Commun. **55**, 87 (1985).
[42] D. R. Miller, *Atomic and Molecular Beam Methods*, edited by G. Scoles (Oxford University Press, New York, 1988), Vol. 1.
[43] J.-C. Nigh and J. J. Valentini, J. Phys. Chem. **91**, 1370 (1987).
[44] L. Herzberg and G. Herzberg, Ap. J. **105**, 353 (1947).
[45] C. E. Moore, *Atomic Energy Levels* NSRDS-NBS 35, Vol. 1 (1971).